Supplement of Atmos. Chem. Phys., 18, 9375–9391, 2018
https://doi.org/10.5194/acp-18-9375-2018-supplement

Atmospheric Chemistry and Physics
Open Access
EGU

Supplement of

Non-polar organic compounds in autumn and winter aerosols in a typical city of eastern China: size distribution and impact of gas–particle partitioning on $PM_{2.5}$ source apportionment

Deming Han et al.

Correspondence to: Jinping Cheng (jpcheng@sjtu.edu.cn)

Section S1. PMF analysis and uncertainty assessment

Positive matrix factorization (PMF) is considered an advanced algorithm among various receptor models, which has been successfully applied for source identification of environmental pollutants (Han et al., 2014; Besis et al., 2016; Han et al., 2018). PMF has the following advantages: each data point is given an uncertainty-weighting; the factors in PMF are not necessarily orthogonal to each other and there is no non-negativity constraint with PMF. In the present study, PMF 5.0 (US EPA) was used to apportion the contributions of different sources to $PM_{2.5}$ in the atmosphere. The matrix X represents an ambient data set in which i represents the number of samples and j the number of chemical species. The goal of multivariate receptor modeling is to identify sources (p), the species profile (f) of each source and the amount of mass (g) contributed by each source to each individual sample as well as the residuals (e_{ij}), as following equation:

$$X_{ij}=\sum_{k=1}^{p} g_{ik}f_{kj}+e_{ij} \quad \text{(S1)}$$

The PMF solution minimizes the objective function Q based on these uncertainties (u):

$$Q=\sum_{i=1}^{n}\sum_{j=1}^{m}\left[\frac{X_{ij}-\sum_{k=1}^{p} g_{ik}f_{kj}}{u_{ij}}\right]^2 \quad \text{(S2)}$$

The input data files of PMF consist of concentrations and uncertainty matrices, and the uncertainty data were calculated as Equation (S3) as suggested by PMF User Guide. The missing values were represented by average values, while measurements below MDL (method detection limit) were replaced by two times of the corresponding MDL values. The "weak" variables were down-weighted, while "bad" variables were omitted form the analysis process.

$$\begin{cases} Unc_i=\frac{5}{6}\times MDL_i & C_i \le MDL_i \\ Unc_i=\sqrt{(C_i\times \text{Error Fraction})^2+\left(\frac{1}{2}\times MDL_i\right)^2} & C_i > MDL_i \end{cases} \quad \text{(S3)}$$

The model was run 20 times with 25 random seeds to determine the stability of goodness-of-fit values.If the number of sources is estimated properly, the theoretical Q value should be approximately the number of degrees of freedom or the total number of data points. Five to eleven factors were examined, and eight factors were found to be the most appropriate and most reasonably interpretable. Q (True) is the goodness-of-fit parameter calculated including all points, while Q (Robust) is the goodness-of-fit parameter calculated excluding points not fit by the model, Q (Robust) and Q (True) were 1,752.4 and 1,812.9, respectively. Additionally, approximately 98% of the residuals calculated by PMF were within the range of -3 to 3, indicating a good fit of simulated results. The factor did not show oblique edges, suggesting there were little rotation for the solution. All these features implied the model simulation result was acceptable.

Section S2. NPOC analysis using TD-GC/MS

Table S1. Abbreviation, P^{o}_{L} and ΔH_0, retention time and quantification ion informationinformation for individual NPOCs

Species	Abb.	P^{o}_{L} [a]	ΔH_0 [b]	Base peak (m/z)	Retention Time (RT)
PAHs					
Fluorene	FLO	1.10E–01	84.9	166	19.25
Phenanthrene	PHE	2.57E–02	88.9	178	24.41
Anthracene	ANT	1.21E–03	99.7	178	24.56
Fluoranthene	FLU	1.60E–03	98.3	166	28.03
Pyrene	PYR	7.60E–04	97.9	202	28.66
Benz[a]anthracene	BaA	3.45E–05	108	228	32.30
Chrysene	CHR	1.36E–06	118.8	228	32.41
Benzo[b]fluoranthene	BbF	1.00E–06	119.2	252	35.32
Benzo[j+k]fluoranthene	BkF	4.66E–06	113	252	35.37
Benzo[a]fluoranthene	BaF	4.66E–05	113		36.13
Benzo[a]pyrene	BaP	7.89E–07	117.9	252	36.01
Indeno[1,2,3-cd]pyrene	IcdP	1.42E–06	124	276	39.22
Dibenz[a,h]+[a,c]anthracene	DahA	4.93E–09	134.1	278	39.00
Benzo[ghi]perylene	BghiP	1.01E–08	129.9	276	38.91
Coronene	COR	3.56E–10	143.2	300	28.71
iso–Alkane					
Pristane	$C_{19}H_{40}$	/ [c]	/	57	23.24
Phytane	$C_{20}H_{42}$	/	/	57	24.69
Hopane					
αβ–Nnorhopane	C_{29}–αβ–NOR–H	2.74E–06	126	191	37.77
αβ–Hopane	C_{30}–αβ–H	1.01E–06	130	191	38.54
αβ–22R–Homohopane	C_{31}—αβ–R	3.85E–07	134	191	39.56
ab 22S–Homohopane	C_{31}—αβ–S	3.85E–07	134	191	39.70
22,29,30–Trisnorhopane	Tm	1.93E–05	117	191	36.63
Sterane					
ααα–20R Cholestane	ααα–20R–C	2.03E–05	121	217	37.29
αββ–20R Cholestane	αββ–20R–C	/	/	218	37.66
αββ–20R24S–Methylcholestane	αββ–20R–MEC	7.60E–06	125	218	36.58
aaa 20R24R–Ethylcholestane	ααα–20R–EC	/	/	217	37.29
αββ–20R24R–Ethylcholestane	αββ–20R–EC	2.84E–06	130	218	37.66
n–Alkanes					
n–Undecane	$C_{11}H_{24}$	/	/	57	12.39
n–Dodecane	$C_{12}H_{26}$	/	/	57	13.92
n–Tridecane	$C_{13}H_{28}$	/	/	57	16.10
n–Tetradecane	$C_{14}H_{30}$	/	/	57	18.15
n–Pentadecane	$C_{15}H_{32}$	/	/	57	20.26
n–Hexadecane	$C_{16}H_{34}$	/	/	57	21.63
n–Heptadecane	$C_{17}H_{36}$	/	/	57	23.15

n–Octadecane	$C_{18}H_{38}$	/	/	57	24.55
n–Nonadecane	$C_{19}H_{40}$	/	/	57	25.87
n–Eicosane	$C_{20}H_{42}$	/	/	57	27.12
n–Heneicosane	$C_{21}H_{44}$	/	/	57	28.33
n–Docosane	$C_{22}H_{46}$	3.24E–03	115	57	29.43
n–Tricosane	$C_{23}H_{48}$	1.22E–03	120	57	30.61
n–Tetracosane	$C_{24}H_{50}$	4.66E–04	124	57	31.55
n–Pentacosane	$C_{25}H_{52}$	1.72E–04	129	57	32.43
n–Hexacosane	$C_{26}H_{54}$	6.59E–05	133	57	33.09
n–Heptacosane	$C_{27}H_{56}$	2.53E–05	137	57	33.36
n–Octacosane	$C_{28}H_{58}$	9.42E–06	142	57	33.50
n–Nonacosane	$C_{29}H_{60}$	3.55E–06	146	57	35.47
n–Triacontane	$C_{30}H_{62}$	1.32E–06	151	57	37.31
n–Hentriacontane	$C_{31}H_{64}$	4.96E–07	155	57	39.24
n–Dotriacontane	$C_{32}H_{66}$	1.93E–07	160	57	37.66
n–Tritriacontane	$C_{33}H_{68}$	7.09E–08	164	57	40.22
n–Tetratriacontane	$C_{34}H_{70}$	2.63E–08	169	57	38.75
n–Pentatriacontane	$C_{35}H_{72}$	1.00E–08	173	57	40.21
n–Hexatriacontane	$C_{36}H_{74}$	3.75E–09	177	57	41.33
n–Hepatriacontane	$C_{37}H_{76}$	1.42E–09	182	57	42.82
n–Octatriacontane	$C_{38}H_{78}$	5.37E–10	186	57	43.55
n–Nonatriacontane	$C_{39}H_{80}$	2.03E–10	191	57	45.13
n–Tetracontane	$C_{40}H_{82}$	7.60E–11	195	57	46.21

[a]: pure compound vapor pressure, unit of Pa at 298 K, cited from And and Hanshaw, 2004, Xie et al., 2013;

[b]: vaporization enthalpy, unit of (KJ mol^{-1}) at 298 K, cited from Xie et al., 2013, Wang et al., 2016;

[c]: "/" means lack of related data.

(a) Pyrene	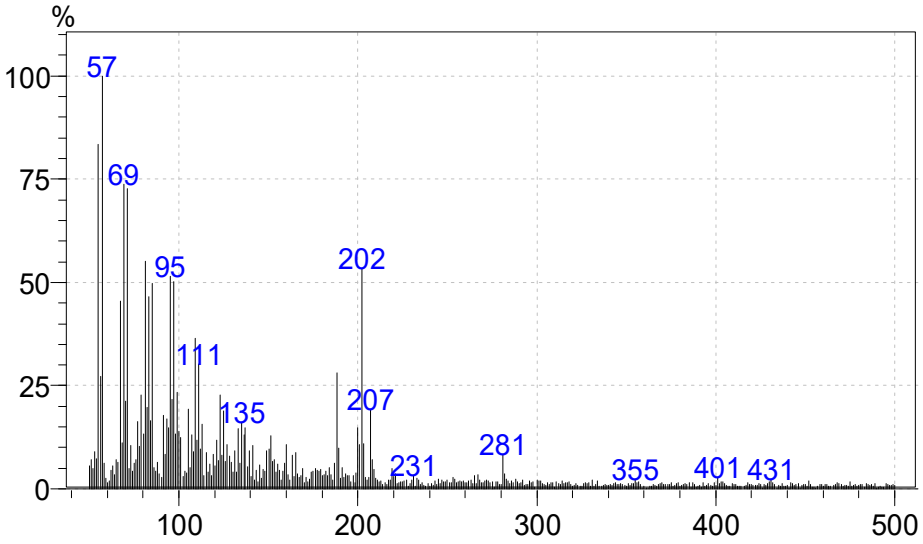
(b) Coronene	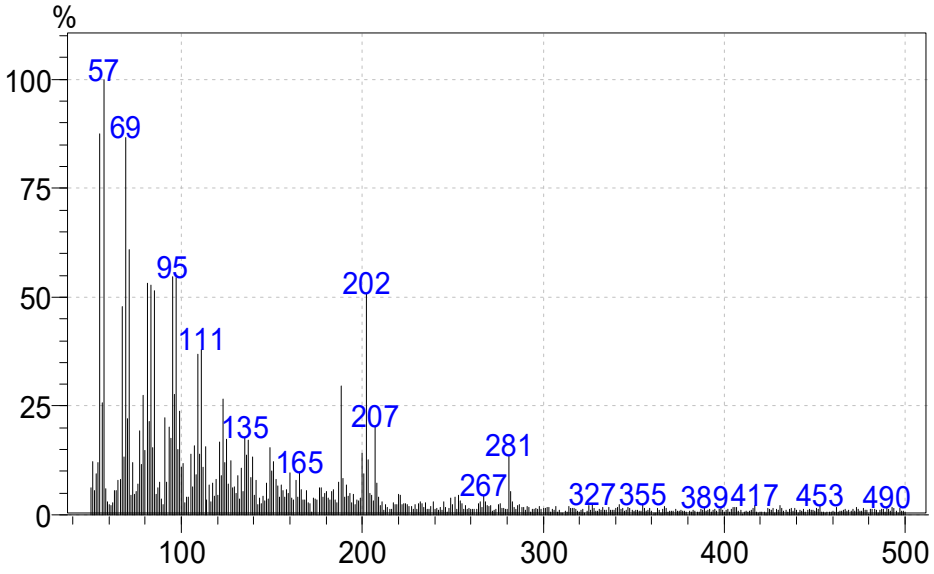

(c) n–Docosane	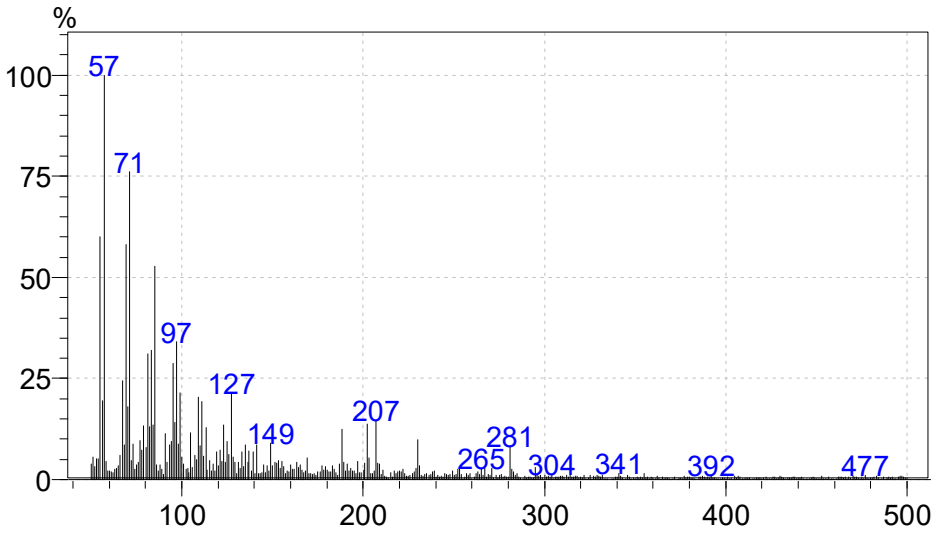
(d) n–Dotriacontane	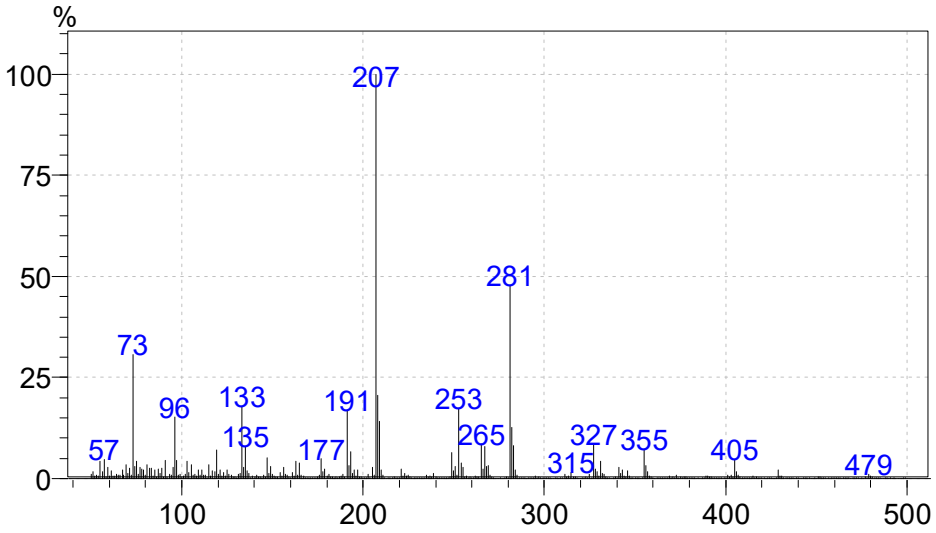

Fig. S1. Mass spectra of the several NPOCs species

Section S3. The measured abundances of NPOCs and MDRs values in each sites

Table S2. Concentrations of NPOCs of each sampling site (ng m^{-3})

	SH	XY	SL	WQ	JJ	Average
PAHs	44.1±10.5	49.7±18.9	47.6±7.6	46.4±13.3	53.7±21.6	45.3±17.6
Alkanes	134.7±56.6	109.5±33.5	93.2±31.9	96.6±31.0	130.4±74.8	112.9±55.1
Hopanes	6.7±4.7	4.4±3.0	5.2±2.5	1.9±1.1	2.8±1.8	4.2±3.0
Steranes	2.5±1.2	3.1±1.8	1.9±0.6	1.1±0.6	1.4±0.8	2.0±1.3
NPOCs	187.9±59.6	166.7±47.3	147.8±33.4	146.0±42.8	188.2±92.1	167.3±68.4
CPI	1.2±0.1	1.3±0.2	1.3±0.2	1.4±0.2	1.3±0.2	1.3±0.2
WNA%	14.6±3.0	16.0±4.5	16.8±4.4	19.3±4.1	17.2±4.7	17.0±4.4
PNA%	85.4±3.0	84.0±4.5	83.2±4.4	80.7±4.1	82.8±4.7	83.0±4.4
C_{max}	C31	C31	C31	C31	C31	C31
ACL	29.2±0.8	28.8±0.7	28.5±0.7	29.7±0.7	29.3±0.8	29.1±0.8
WAX_{cn}	20.3±11.2	16.8±5.8	15.6±6.6	18.3±6.3	20.9±10.9	17.3±9.1

Section S4. Gas-particle partitioning for NPOCs

To further evaluate gas-particle partitioning of NPOCs, φ values were compared with predicted ones by Jungle–Pankow model (Fig. S2). The φ values of LMW PAHs, short chain n-alkanes, $\log P^{o}_{L} > -5$ hopanes and steranes, were underpredicted by Jungle–Pankow model. However, the φ values predicted by Jungle–Pankow model agreed well with the calculated ones for HMW PAHs and long chain n-alkanes. Underestimation of φ values of PAHs by Jungle–Pankow model compared with the filed measured ones were also reported by He and Balasubramanian, (2009), and they attributed the discrepancy to the higher OM fractions in real environment than that adopted by the model.

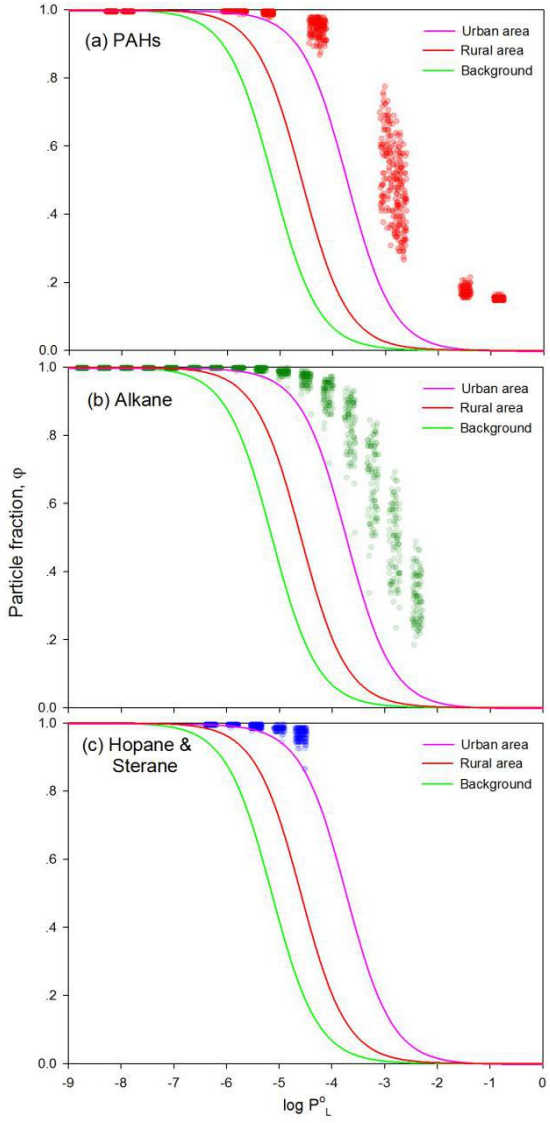

Fig. S2. Comparison of φ values between the measured and predicted results from Jungle–Pankow model

Partition between gas and particle phases was evaluated by regression of K_p and subcooled vapor pressure P^o_L (Pa), using the following equation:

$$\log K_p = m_r \log P^o_L + b_r \qquad \text{(S4)}$$

Useful information pertaining to gas–particle partitioning can be drawn from the regressed parameter mr and br. The calculated and Jungle-Pankow model predicted logK_p values were depicted in fig. S1. It can be clearly that the model predicted logK_p values were a bit lower than the empirical calculated ones, regardless of NPOCs species.

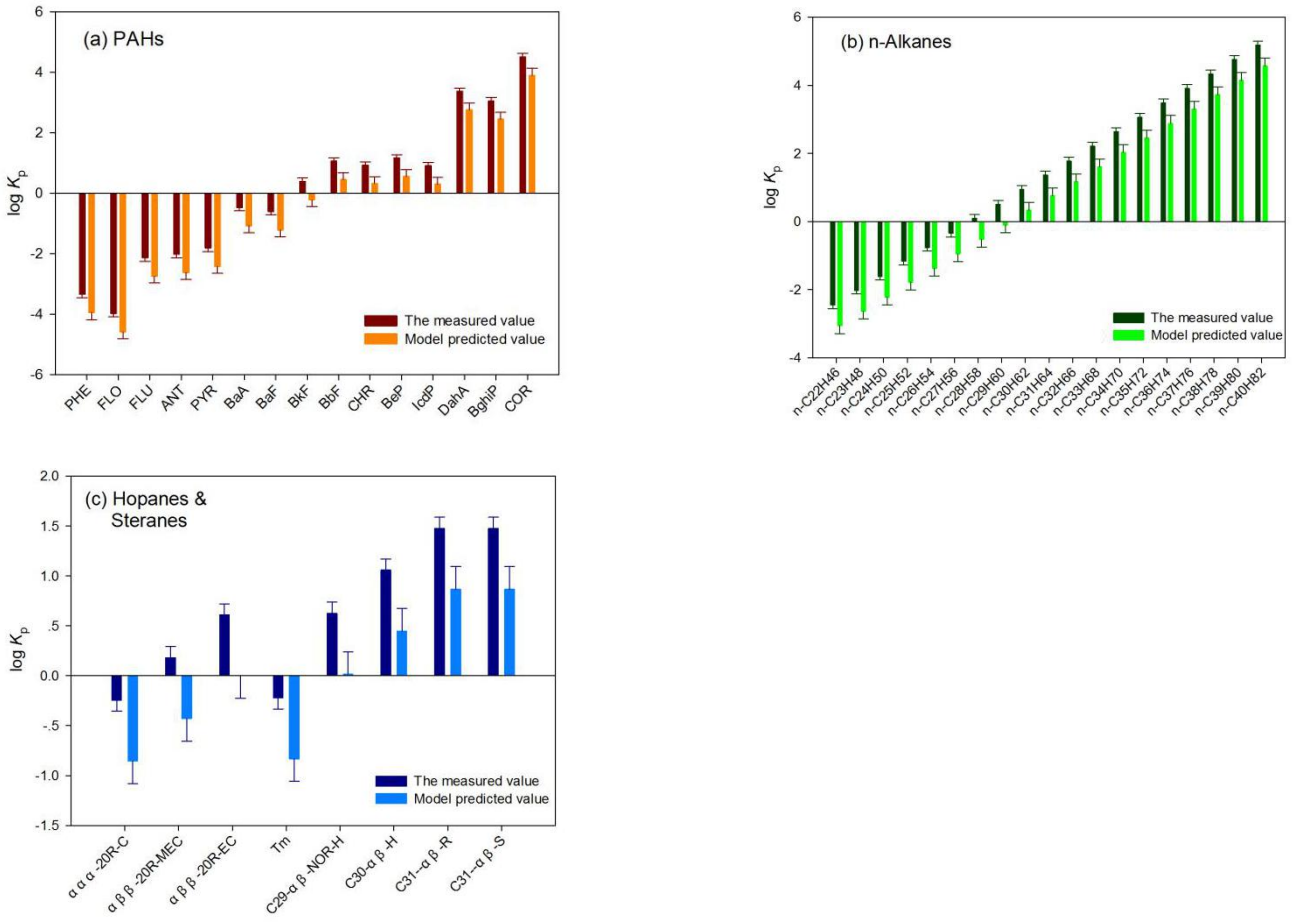

Fig. S3. Comparisons of the measured and model predicted φ values

Section S5. Source distributions extracted from single particle phase and gas-particle phases NPOCs as input data

The contributions of individual source to the total concentrations for both PMF_P and PMF_T models were compared in Fig. S4. Secondary aerosol formation was the largest contributor, occupied 24.7% and 21.8% of the single and the total concentrations in PMF_P and PMF_T, respectively. Vehicles exhaust, biomass burning, dust, industrial emission and coal combustion were major contributors, occupying of 12.5%/15.0%, 12.7%/15.7%, 8.9%/11.0%, 13.8%/11.9% and 17.5%/12.4% in PMF_P/PMF_T, respectively. For the light NPOCs source, the contributions of PMF_P and PMF_T models were 3.7% and 5.6% respectively, with a relatively high contribution for PMF_T but much smaller in the PMF_P.

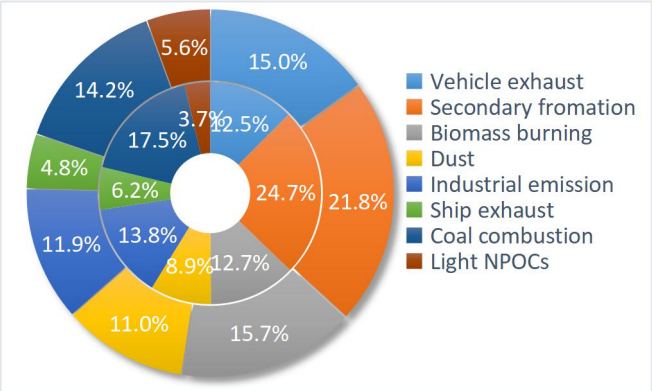

Fig. S4. Contributions of eight sources resolved by PMF (inner circular ring for single particle bound NPOCs, the outer circular ring for the total NPOCs)

Reference

Besis, A., Voutsa, D., Samara, C. (2016). Atmospheric occurrence and gas-particle partitioning of PBDEs at industrial, urban and suburban sites of Thessaloniki, Northern Greece: implications for human health. Environ. Pollut. 215, 113-124.

Feng, J., Hu, M., Chan, C. K., Lau, P. S., Fang, M., He, L., and Tang, X.: A comparative study of the organic matter in PM2.5 from three Chinese megacities in three different climatic zones, Atmos. Environ., 40, 3983-3994, 2006.

Han, D., Ye, L., Zhang, C., Li, W., Ma, W.L., Li, Y. (2014). Gas-particle partitioning of polychlorinated biphenyls in air of Xi'an City. China Environ. Sci. 34 (10), 2466-2471.

Han D, Zhang J, Hu Z, Ma Y, Duan Y, Han Y, Chen X, Zhou Y, Cheng J, Wang W. (2018). Particulate mercury in ambient air in Shanghai, China: Size-specific distribution, gaseparticle partitioning, and association with carbonaceous composition. Environ. Pollut. 238, 543-553

Hien, T. T., Le, T. T., Kameda, T., Takenaka, N., and Bandow, H.: Distribution characteristics of polycyclic aromatic hydrocarbons with particle size in urban aerosols at the roadside in Ho Chi Minh City, Vietnam, Atmos. Environ., 41, 1575-1586, 2007.

Ho, S. S., and Yu, J. Z.: In-injection port thermal desorption and subsequent gas chromatography-mass spectrometric analysis of polycyclic aromatic hydrocarbons and n-alkanes in atmospheric aerosol samples, J. Chromatography A, 1059, 121, 2004.

Wang, Q., Feng, Y., Huang, X. H. H., Griffith, S. M., Zhang, T., Zhang, Q., Wu, D., and Yu, J. Z.: Non-polar organic compounds as PM2.5 source tracers: Investigation of their sources and degradation in the Pearl River Delta, China, J. Geophy. Res. Atmos, 2016.